

A Search for Outstanding Sources of PeV Cosmic Rays: Cassiopeia A, the Crab Nebula, the Monogem Ring | But How About M 33 and the Virgo Cluster?

G. V. Kulikov, M. Yu. Zotov

D. V. Skobeltsyn Institute of Nuclear Physics
Moscow State University, Moscow 119992, Russia
fkulikov, zotovg@eas.sinp.msu.ru

April 22, 2005

Abstract

We study arrival directions of $1.4 \cdot 10^6$ extensive air showers (EAS) registered with the EAS-1000 Prototype Array in the energy range $0.1\text{--}10$ PeV. By applying an iterative algorithm that provides uniform distribution of the data with respect to sidereal time and azimuthal angles, we find a number of zones with excessive flux of cosmic rays (CRs) at ~ 3 level. We compare locations of the zones with positions of galactic supernova remnants (SNRs), pulsars, open star clusters, OB-associations, and regions of ionized hydrogen and find remarkable coincidences, which may witness in favour of the hypothesis that certain objects of these types, including the SNRs Cassiopeia A, the Crab Nebula, the Monogem Ring and some other, provide a noticeable contribution to the flux of CRs in the PeV range of energies. In addition, we find certain signs of a contribution from the M 33 galaxy and a number of comparatively nearby groups of active galactic nuclei and interacting galaxies, in particular those in the Virgo cluster of galaxies. The results also provide some hints for a search of possible sources of ultra-high energy (UHE) cosmic rays and support an earlier idea that a part of both UHE and PeV CRs may originate from the same astrophysical objects.

TM TOW TDI

The Perl community mantra

1. Introduction

In spite of the fact that cosmic rays were discovered more than 90 years ago [1], the problem of their origin for energies greater than 100 TeV remains unsolved. One of the important directions in numerous approaches to the problem is an analysis of arrival directions of CRs. Such an analysis has been performed with the data sets obtained with practically all extensive air shower experiments, see [2], [3], [4], and [5] for the latest reports and a list of references. One of the main results of the majority of these investigations is that there is no significant anisotropy in the energy range $0.1\text{--}100$ PeV [6].

Another intriguing and long-standing problem in cosmic ray physics is the so called ‘knee’ around $3 \cdot 10^5$ eV in the CR energy spectrum [7]. The knee is a point where the spectral index of the all-particle differential power-law spectrum changes from approximately -2.7 to -3.1 . There are a number of models aimed to explain this feature (as well as the origin of CRs), see, e.g., [8], [9], [10], and [11] for a number of recent works and [12] for an earlier review. Still, none of them seems to be fully established yet. One of the modern ‘astrophysical’ approaches to the problem is the ‘single source model’ by Erlykin and Wolfendale [13]. The model explains the knee as a result of a contribution from one comparatively recent (~ 100 kyr) and nearby (~ 300 pc) supernova remnant accompanied by a pulsar. Evidently, an analysis of arrival directions of CRs in the energy range around the knee can be useful as a (partial) experimental test of the model.

An interest to the single source model has recently received an additional impulse after the discovery that the pulsar PSR B0656+14 is located near the center of the Monogem Ring SNR at the distance of about 290 pc [14]. Since then, there has been a number of reports on the analysis of the flux of cosmic

There’s More Than One Way To Do It.

rays with energies around the knee from the direction to this source. Interestingly, some of the results are controversial. Namely, Chilingarian et al. [2] and Benko et al. [4] find a significant excess of EAS from zones near the pulsar PSR B0656+14 while the KASCADE collaboration considers this excess as negligible [3]. To shed an additional light on the situation, we perform an analysis of arrival directions of EAS registered with the EAS{1000 Prototype Array, which has been operating at Moscow State University. Unfortunately, the energy range covered by the array is not sufficient for a comprehensive investigation of arrival directions of EAS around the knee since it mostly covers a range of energies just below the knee. Still, we find the first results of this work sufficiently interesting and promising to report.

The most important result is the discovery of a whole number of zones with an excessive flux (ZEF) of CRs around 1 PeV at 3 level. The majority of the ZEF correspond to the locations of galactic SNRs, pulsars, open star clusters, OB-associations, and regions of ionized hydrogen. In particular, we confirm the conclusions of Chilingarian et al. [2] and Benko et al. [4] on the excessive flux of CRs from the direction to the Monogem Ring. Still, a number of the zones have no or just a few objects of the above types nearby. We find that one of these 'empty' or 'under filled' ZEF contains the M33 galaxy inside, while the majority of others have neighbouring active galactic nuclei (AGN) and/or interacting galaxies at redshifts $z < 0.01$ with a big group of them located in the Virgo cluster of galaxies. In addition, we find a few remarkable coincidences between positions of the ZEF and arrival directions of ultra-high energy cosmic rays registered with the AGASA array [15].

2. Experimental Data

The EAS{1000 Prototype Array consists of eight detectors situated in the central part of the EAS MSU array along longer sides of the 64m × 22m rectangle [16]. The array is located at 37°32.5'E, 55°41.9'N at approximately 200 m above sea level.

The data set under consideration includes 1,668,489 EAS registered during 203 days of operation of the array in the period from August 30, 1997, till February 1, 1999. The arrival directions are determined for 1,366,010 EAS. A number N_e of charged particles (electrons) is found for 826,921 EAS. It happens that N_e of 95.2% of showers with zenith angles $\leq 45^\circ$ lie in the range $10^4 \{1.1 \cdot 10^5$ particles with $N_e = 1.2 \cdot 10^5$ and the median value equal to $6 \cdot 10^4$. Thus we estimate that the overwhelming majority of primary cosmic rays that give life to the EAS in the data set have energies in the range $E \sim 0.1 \{ 10$ PeV. Still, only 92,212 EAS have $N_e > 3 \cdot 10^5$. Thus one may treat the data set as mostly covering an interval of energies just below the knee.

3. Method of Data Analysis

Perhaps the majority of investigations of anisotropy rely on the Rayleigh method for the calculation of the amplitude and the phase of the first and (sometimes) the second harmonics [6]. The method by itself is based on the Fourier transform. This does not seem to be a fruitful approach in all situations. For example, one can easily check that an analysis of the one-dimensional Fourier spectrum does not necessarily give reliable results if the amplitude of a periodic signal is less than or of the order of 0.3% of that of noise for a sample that consists of 10^6 points. Thus we expect that a similar situation can take place in the case of anisotropy analysis. This makes us develop another approach, which may be considered as an advanced version of the method employed in [17]. The algorithm consists of three main steps: data alignment, data averaging, and selection of ZEF.

Step 1: Data Alignment. The main aim of the step is to obtain a data set that consists of EAS with a uniform distribution of azimuthal angles and sidereal times.

1. Fix values θ and s of the width of bins in histograms of θ and s . Produce a histogram of N_i . By N_i denote the number of EAS in the i th bin.
2. In the histogram of θ , find a bin with the least number of showers, N_{min} . At random, exclude $(N_i - N_{min})$ showers from each bin.
3. Obtain a histogram of s for the remaining data set. With this histogram, perform an 'alignment' of data exactly as in item 2.
4. Produce a histogram of θ for the data set obtained in item 3. Finish the procedure if

$$\max_i N_i - N \leq 2.5; \text{ and } \max_i N_i - N < 3; \quad (1)$$

where N is the mean number of EAS in the bins of the histogram, and σ is the standard deviation. Otherwise, repeat items 2 and 3.

Conditions (1) were chosen after comparing a number of empirical criteria. In practice, the second inequality is always fulfilled earlier than the first one and may be omitted.

We stress that the data set obtained as a result of Step 1 contains equal number of EAS in each bin of the histogram of the sidereal times thus providing uniform distribution of the data with respect to s at the chosen scales. The same is approximately true for the distribution with respect to α .

For the data set under consideration, Step 1 leads to an exclusion of up to 20% of all EAS in the data set. It is obvious that results of an analysis of the 'aligned' data set will strongly depend on the choice of the excluded EAS. Hence we come to the necessity to implement Step 1 numerous times thus obtaining a family of 'aligned' data sets. Each time, an independent sample of EAS is excluded from the whole data set.

Step 2: Data Averaging. For each 'aligned' data set, produce a map of the distribution of EAS arrival directions in equatorial coordinates. Each map consists of $1^\circ \times 1^\circ$ cells ('unit' cells) and covers the complete observable region with the right ascension $= 0:::24$ h and the declination $> 13^\circ$. For each cell in all maps, a number of EAS inside the cell is found. After this, an averaged map is produced.

At this point, we are ready to join unit cells into larger ones and look for cells with an excessive flux (CEF) of cosmic rays. We do not analyse unit cells because it seems unlikely that charged particles of PeV energies preserve directions to their sources with such precision.

Step 3: Selection of CEF.

1. Divide the averaged map into strips of equal width $\Delta\delta = 3^\circ$ in the declination. The boundaries of strips of equal width are shifted with respect to each other by 1° .
2. Split each strip into cells of equal width $\Delta\alpha = 3^\circ$. For each strip and each partition into cells, find the mean number N of EAS for all cells within the strip and the standard deviation σ . Mark a cell with N EAS inside as having an excessive CR flux if $N > N + 3\sigma$, and $N > 10$.

Remark 1. It often happens that the algorithm selects a number of intersecting or overlapping CEF, so that it is inconvenient to discuss each of them separately. Instead, we shall discuss zones of excessive flux (ZEF), by which we mean sets of intersecting or overlapping CEF. For simplicity, we shall use this term even in case a ZEF consists of a single cell.

Remark 2. It is not important for the algorithm how the values of $\Delta\alpha$ and $\Delta\delta$ are chosen. The maps of ZEF discussed below are combined of cells such that $\Delta\alpha \Delta\delta$ equals a rounded value of $\Delta\alpha_0 \Delta\delta_0 = \cos \delta_0$, where δ_0 is the mean value of the declination for the strip. This guarantees that cells with the same $\Delta\alpha \Delta\delta$ but located at different declination, have an approximately equal area. This is a traditional choice for similar investigations. In what follows, we call these cells 'regular'. Still, there are no reasons to restrict the analysis to regular cells only. Thus, we have also studied cells with arbitrary values of $\Delta\alpha \Delta\delta$ providing that they are integer dividers of 360. These 'irregular' cells are in no sense worse than 'regular' ones. More than this, in some cases an employment of irregular cells allows one to find CEF that are more pronounced than their regular counterparts in the sense of deviation from N . On the other hand, for any regular CEF, there is an irregular one with the same or close size. A number of interesting irregular CEF will be presented below.

It is important to mention that all CEF have a neighbourhood with a flux of CRs that is higher than the average for the strip though it does not reach the level of 3σ . In our opinion, this means that CEF are not just random fluctuations of the level of the flux caused by the algorithm.

Remark 3. The rule used to choose CEF implicitly assumes that the number of EAS within cells of any strip obey the Gaussian distribution with the corresponding parameters. The hypothesis seems to be possible since these numbers are generically non-integer due to the averaging of the data set. Nevertheless, one may choose another rule to select CEF.

Remark 4. An analysis of the algorithm described above has revealed that maps of 'averaged' EAS arrival directions obtained with 100 cycles of alignment differ very little from each other. Still, in order to make our conclusions even more robust, we present results obtained for 1000 cycles. To perform calculations, we have employed GNU Octave [18] running in Linux.

Remark 5. In what follows, we present results obtained for $\Delta\alpha = 20^\circ$ and $\Delta\delta = 3^\circ$ h, which provide a comparatively small number of excluded EAS and an acceptable speed of the algorithm. An analysis of

averaged maps obtained for different values of α and δ in the range $\alpha = 10^\circ \dots 30^\circ$ and $\delta = 1^\circ \dots 3^\circ$ and cells of the size $5^\circ \times 5^\circ$ has revealed that the results differ from those obtained for $\alpha = 20^\circ$ and $\delta = 3^\circ$ by at most 0.1. Thus one may expect that the condition $N_{\text{EAS}} \geq 3$ used to select CEF guarantees that $N_{\text{EAS}} \geq 3$ for other sensible values of α , δ , and sizes of cells.

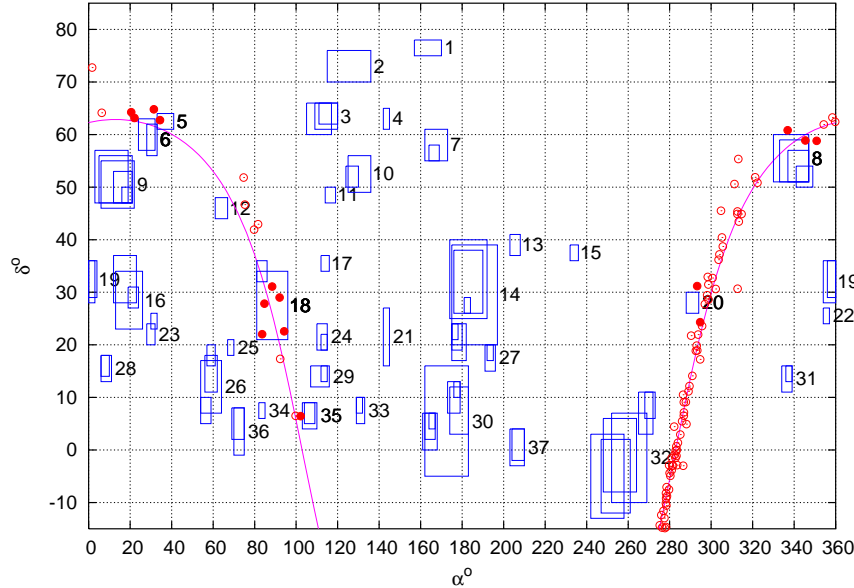


Figure 1: Zones with excessive flux of cosmic rays (rectangles) and galactic SNRs () in the region 15° . The ZEF are numbered from top to bottom according to the values of their upper boundaries. The curves show the galactic plane. Filled circles show SNRs located within 2°-neighbourhoods of the ZEF.

4. Analysis of the Data Set

The above procedure applied to the whole data set resulted in the 'averaged' set of 1,134,325 EAS and 193 regular and an even greater number of irregular CEF. The regular CEF and a number of irregular CEF were joined into 37 ZEF, see Fig. 1. A number of CEF are embedded into each other or shifted with respect to each other by 1°. To make this and the following figures as clear as possible, we omit some of these CEF but show their joint boundaries instead.

An important question is how many EAS are there inside ZEF? Below we shall give exact numbers but it may be useful to remember the following: (i) any CEF contains at least 10 EAS; (ii) any unit cell located in the region $26^\circ \leq \delta \leq 80^\circ$ contains > 10 EAS; (iii) the mean number of EAS inside unit cells located in the region $19^\circ \leq \delta \leq 85^\circ$ is greater than 9; (iv) $m_{\text{min}} = 12.38$ but there are only 50 EAS with $\delta < 0^\circ$.

4.1. Galactic SNRs. Let us begin an analysis of positions of possible CR sources with galactic supernova remnants. For this purpose, we use the January 2004 version of the D. Green Catalogue [19].

Figure 1 shows positions of 96 galactic SNRs located in the region 15° . (The Monogem Ring remnant is not shown since it is not present in the main list of [19].) It happens that 15 SNRs lie inside or at angular distances $\leq 2^\circ$ from the nearest ZEF. Namely,

ZEF No. 5 has the SNR G 132.7+1.3 (HB 3) inside and the remnant G 130.7+3.1 (SN 1181) located at the angular distance $= 1.1^\circ$;

ZEF No. 6 has the SNR G 127.1+0.5 (R 5) at $\delta = 0.9^\circ$, the SNR G 126.2+1.6 at $\delta = 2.0^\circ$, and the remnants associated with ZEF No. 5 at $\delta = 1.0^\circ$ and $\delta = 1.8^\circ$ respectively;

ZEF No. 8 has the SNRs G 109.1-1.0 (CTB 109) inside, G 106.3+2.7 at $\delta = 0.8^\circ$, and G 111.7-2.1 (Cassiopeia A) at the angular distance $= 2.0^\circ$;

ZEF No. 18 has five SNRs inside: G 179.0+2.6, G 180.0-1.7 (S147), G 182.4+4.3, G 184.6-5.8 (the Crab Nebula, SN 1054), and G 189.1+3.0 (IC 443);

ZEF No. 20 has the SNR G 65.3+ 5.7, located at $\alpha = 1.2$ and the SNR G 59.8+ 1.2 at $\alpha = 1.8$.
ZEF No. 35 has the SNR G 206.9+ 2.3 (PKS 0646+ 06), located at $\alpha = 0.8$.

Table 1. Some parameters of the ZEF with galactic SNRs inside or at angular distances $\leq 2^\circ$.
Notation by columns: 'ZEF' is the number of the ZEF as shown in Fig. 1 (letters 'Ir' mark irregular CEF), and α and δ are the ranges of values of the right ascension and the declination for the listed cells respectively, N is the number of EAS in the cell, \bar{N} is the mean number of EAS in the corresponding strip for the given value of α , σ is the standard deviation for the strip, $D = (N - \bar{N})/\sigma$, i.e., the deviation of N from \bar{N} in units of σ .

ZEF	α	δ	N	\bar{N}	σ	D
5 (Ir)	33 :: 41	61 :: 64	1673.2	1546.5	39.10	3.24
6 (Ir)	24 :: 32	57 :: 63	3467.0	3297.0	54.09	3.14
	29 :: 32	59 :: 62	703.6	615.8	23.31	3.76
	29 :: 33	56 :: 62	1804.2	1680.8	38.03	3.24
8	331 :: 347	51 :: 60	10883.4	10546.1	105.47	3.20
	342 :: 348	50 :: 54	1969.3	1818.6	41.45	3.64
18	81 :: 86	32 :: 36	984.9	901.8	26.69	3.11
	81 :: 96	21 :: 34	5445.8	5266.3	57.48	3.12
20 (Ir)	288 :: 294	26 :: 30	734.5	660.7	21.72	3.39
35	103 :: 108	4 :: 9	24.6	14.0	3.38	3.14
	104 :: 108	5 :: 9	20.5	10.0	3.14	3.34

Notice that a number of these SNRs are widely discussed in literature as possible sources of CRs in the region of the knee. Among them, Cassiopeia A (see, e.g., [20], [21] and references therein), the Crab Nebula, and the SNRs S147 and G 65.3+ 5.7 [22], [23].

An extension of the selection zone up to the angular distance 3° adds two more SNRs to the list, namely G 59.5+ 0.1 and G 63.7+ 1.1 both lying near ZEF No. 20. Another prominent SNR, the Monoceros Nebula, is located at $\alpha = 3.2$ to the west from ZEF No. 35.

Table 1 contains some parameters of the discussed ZEF. Among them, ZEF No. 5, 6, and 20 are made of irregular cells. In the boundaries shown in Fig. 1, ZEF No. 6, 8 and 35 consist of 18, 10, and 4 CEF respectively. For the sake of brevity, only the most interesting of them are presented in Table 1. Notice that all these ZEF except No. 35 lie in the region with a high density of EAS per unit cell and thus contain hundreds and even thousands of showers.

4.2. Pulsars. Figure 2 shows the mutual position of the ZEF and pulsars known in the region $\alpha \leq 15$ [24], version of October 11, 2004. Forty-six of these 640 pulsars lie inside the ZEF, other 34 pulsars lie at angular distances $\leq 2^\circ$ from the boundaries of the nearest ZEF. As one can see from the figure, the list of zones with 'neighbouring' pulsars consists of 21 ZEF: No. 2 {6, 8, 9, 14, 16, 18, 20, 21, 26, and 29} 36. Notice that all ZEF discussed above in connection with galactic SNRs belong to the list. Some parameters of the ZEF 'selected' by pulsars are presented in Tables 2 and 3. The biggest number of pulsars within 2° -neighbourhoods are found for ZEF No. 32 (26 PSRs), No. 8 and 18 (8 PSRs), No. 6 and No. 20 (7 and 6 PSRs respectively). Each of ZEF No. 5, 9, 14, and 21 has four neighbouring pulsars. It is interesting to mention that 13 of 640 pulsars in the region $\alpha \leq 15$ are associated with galactic SNRs. Five of them lie within 2° from the ZEF.

We have already mentioned the pulsar PSR B0656+ 14 in connection with the single-source model by Eriykin and Wolfendale [13]. The pulsar has equatorial coordinates $\alpha = 104.95$, $\delta = 14.24$ and is located close in projection to the center of the Monogem Ring SNR [14]. As is clear from Fig. 2 and Table 3, the pulsar lies at the angular distance $\alpha = 2.05$ from the left boundary of the outer cell of ZEF No. 29. This is an irregular cell of the size 9×4 . The interior (regular) 3×3 cell is located at $\alpha = 7.05$ from the pulsar.

The interior cell is especially interesting in connection with the article by Chilingarian et al. [2], in which arrival directions of more than 2×10^5 EAS with the size $N_e > 10^5$ detected by the MAKET-ANI experiment have been analysed. As a result, a 3×3 CEF located at $\alpha = 111 :: 114$, $\delta = 12.5 :: 15.5$

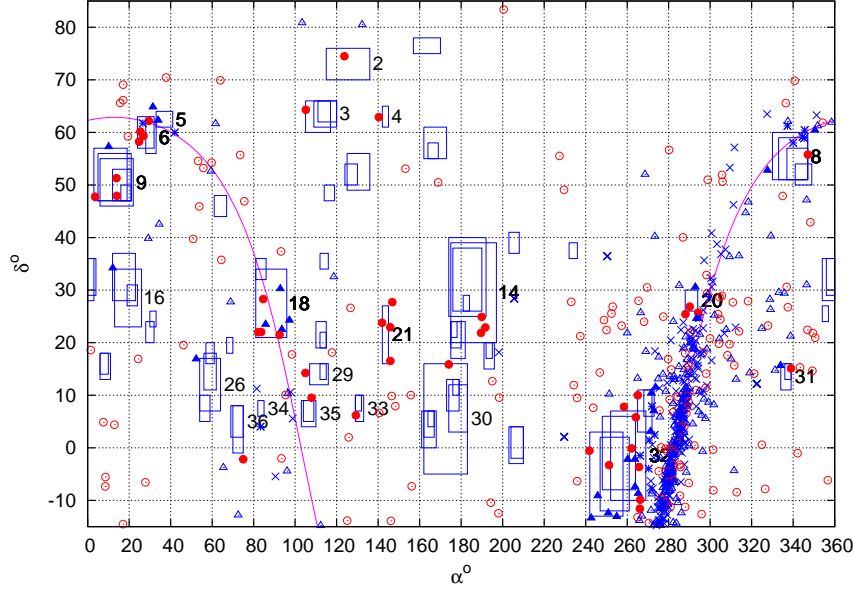


Figure 2: The ZEF and pulsars in the region 15 [24]. Different symbols denote pulsars located at different distances d from the solar system: \square $d \leq 3$ kpc, \square $3 < d \leq 6$ kpc, \square $d > 6$ kpc or the distance is unknown. Filled circles, filled triangles, and asterisks (*) are used respectively to show pulsars located within 2°-neighbourhoods of the ZEF.

has been found. Evidently, this CEF is very close to the interior cell in ZEF No. 29. Here one should take into account that (i) we have not studied cells with boundaries located at non-integer values of α or δ , and (ii) Chilingarian et al. have not studied cells with the size larger than $3^\circ \times 3^\circ$. Thus we think this is a remarkable coincidence of the results, obtained in different experiments and by different methods of data analysis.

It is worth mentioning that the Monogem Ring remnant covers a huge region with the diameter of approximately 25° with its most pronounced part being at the right hand side of the circle, see the figure in [14]. (To the contrary to our figures, Thorsett et al. [14] use the grid with bigger values of α located at the left-hand side of the figure.) Thus it is clear that ZEF No. 24 and 35 are intersected by the most pronounced part of the Monogem Ring, cf. Fig. 1.

As one can see in Fig. 2, two other pulsars are located comparatively close to ZEF No. 29. These are J0711+0931, located on the top of ZEF No. 35, ($d = 2.39$ kpc, $\alpha = 2.5^\circ$ from ZEF No. 29) and J0751+1807 ($d = 2.02$ kpc, $\alpha = 2.7^\circ$), which lies to the NE from ZEF No. 29. (This pulsar looks to be located closer to ZEF No. 24 but in fact the corresponding angular distance equals nearly 2.8° .)

Another interesting issue is the distribution of distances d to the 'neighbouring' pulsars. As we have already mentioned above, there are 80 pulsars that belong to the 2°-neighbourhoods of the ZEF. One of them lies at $d > 10$ kpc. Distances to four other pulsars are unknown. The remaining 75 pulsars are located at $d \leq 10$ kpc. As for the whole set of 640 pulsars in the region 15, 582 of them have $d \leq 10$ kpc, and $d > 10$ kpc for 49 pulsars. Distances to the remaining 9 pulsars are unknown. Thus let us take a look at the distribution of distances $d \leq 10$ kpc. To do this, define

$$K(d) = \frac{582 N_{\text{PSR}}^{\text{close}}(d)}{75 N_{\text{PSR}}^{\text{all}}(d)}; \quad (2)$$

where $N_{\text{PSR}}^{\text{close}}$ and $N_{\text{PSR}}^{\text{all}}$ are the number of pulsars within the corresponding intervals of d for the 2°-neighbourhoods of ZEF and for all pulsars respectively. A value $K = 1$ corresponds to the case when a fraction of neighbouring pulsars at the given interval of d equals that for the whole set of pulsars.

Figure 3 shows the behavior of $K(d)$ in 0.5-kpc intervals. It is clearly seen that a fraction of neighbouring pulsars with $d > 8$ kpc is negligibly small. On the other hand, $K > 1$ for $d \leq 4$ kpc with the most pronounced

Table 2. Some parameters of the ZEF with pulsars inside. For composite ZEF made of multiple CEF, the corresponding number is given in parenthesis after the number of the zone. See Table 1 for other notation and parameters of ZEF No. 5, 6, 8, 18, and 20.

ZEF			N	N		D
2	115 :::136	70 :::76	4724.2	4558.6	52.77	3.14
3 Ir	109 :::120	61 :::66	3580.6	3401.5	54.99	3.26
	111 :::120	62 :::66	2315.8	2184.0	42.52	3.10
	105 :::117	60 :::66	4765.7	4536.3	73.65	3.11
9 (16)	3 :::19	47 :::57	12266.9	11977.8	93.13	3.10
	6 :::20	47 :::56	9744.3	9458.4	85.12	3.36
	7 :::21	46 :::55	9748.3	9478.5	74.96	3.60
	10 :::21	48 :::55	6027.6	5820.7	63.22	3.27
	15 :::21	47 :::51	1922.1	1808.1	33.86	3.37
14 (14)	175 :::180	19 :::24	379.5	327.1	14.59	3.60
	175 :::197	20 :::39	14014.1	13689.8	102.80	3.15
	176 :::190	26 :::38	6770.4	6564.0	64.96	3.18
	181 :::184	26 :::29	285.9	236.5	14.38	3.43
16 (6)	12 :::23	28 :::37	4136.0	3999.7	41.95	3.25
	13 :::26	23 :::34	4342.6	4203.5	43.34	3.21
	19 :::24	27 :::31	677.1	604.7	22.14	3.27
	20 :::23	28 :::31	331.5	283.0	14.22	3.42
30 (19)	161 :::167	1 :::7	22.0	10.2	3.01	3.90
	162 :::183	5 :::16	529.5	472.4	18.32	3.11
	163 :::168	2 :::7	16.9	7.9	2.51	3.58
	175 :::183	5 :::13	107.2	78.4	8.59	3.35
	176 :::179	10 :::13	32.6	18.4	4.24	3.36
31 (4)	334 :::339	11 :::16	112.7	81.8	9.05	3.42
	336 :::339	11 :::14	40.7	22.9	4.54	3.93
	336 :::339	13 :::16	51.5	35.2	5.08	3.21
32 (68)	242 :::258	13 :::3	15.1	7.4	2.38	3.26
	247 :::262	9 :::6	34.9	20.6	4.41	3.24
	248 :::262	8 :::6	34.0	19.4	4.15	3.52
	250 :::262	6 :::6	29.6	16.4	3.90	3.39
	252 :::269	10 :::7	49.0	32.8	4.97	3.26
	265 :::272	4 :::11	58.9	38.5	5.92	3.45
	268 :::272	7 :::11	29.7	16.9	3.74	3.41
33 Ir	129 :::132	7 :::10	17.2	8.2	2.69	3.36
	129 :::133	5 :::10	25.7	14.7	3.54	3.11

bins located at $1.5 < d \leq 2$ kpc and $d \leq 0.5$ kpc.¹ In our opinion, the latter fact can witness in favour of the hypothesis that a noticeable fraction of the overall flux of CRs near the knee is produced by nearby pulsars.

Totally, we find five pulsars located at distances $d \leq 0.5$ kpc from the solar system that belong to the 2-neighbourhoods of ZEF:

PSR B0656+14 at $d = 2$ from ZEF No. 29 ($d = 0.29$ kpc);

PSR J1136+1551 inside ZEF No. 30 ($d = 0.36$ kpc), also at $d = 1.5$ from ZEF No. 14;

PSR J1744-1134 at $d = 1.6$ from ZEF No. 32 ($d = 0.36$ kpc);

PSR J0814+7429 inside ZEF No. 2 ($d = 0.43$ kpc);

¹ The ATNF database [24] gives two basic values of distance to a pulsar: the best estimate of the pulsar distance and the distance based on the Taylor & Cordes electron density model [25]. For definiteness, we use the best estimate. Nevertheless, our results do not change qualitatively if the second value is used. In this case, the highest bins correspond to distances $d \leq 0.5$ kpc and $1.5 < d \leq 2.5$ kpc.

Table 3. Some parameters of the ZEF with pulsars at angular distances $0 < \theta < 3^\circ$. See Table 1 for notation and parameters of ZEF No. 35.

ZEF			N	N		D
4 (Ir)	142 :: 145	61 :: 65	846.2	757.3	25.57	3.47
17	112 :: 116	34 :: 37	658.1	590.5	21.76	3.11
21 (Ir)	142 :: 145	16 :: 27	508.8	448.9	18.35	3.26
24	110 :: 115	19 :: 24	374.6	327.1	14.59	3.26
	112 :: 115	19 :: 22	130.4	100.6	8.75	3.41
26 (19)	54 :: 59	5 :: 10	32.5	18.4	4.46	3.17
	54 :: 64	7 :: 17	310.8	262.7	15.02	3.20
	56 :: 62	11 :: 17	173.2	132.2	11.80	3.47
	57 :: 61	16 :: 20	153.5	121.3	10.11	3.18
	58 :: 62	13 :: 17	100.5	69.7	8.28	3.72
27	192 :: 195	17 :: 20	102.1	73.9	8.19	3.44
Ir	192 :: 196	15 :: 20	179.2	140.5	11.26	3.44
Ir	191 :: 195	15 :: 20	177.3	140.5	11.66	3.15
29	112 :: 115	13 :: 16	52.5	35.2	5.04	3.43
Ir	107 :: 116	12 :: 16	160.1	129.4	9.36	3.28
34	82 :: 85	6 :: 9	13.8	6.3	2.30	3.28
36 (2)	69 :: 75	2 :: 8	25.1	14.0	3.47	3.20
Ir	70 :: 75	1 :: 8	23.6	12.9	3.41	3.15

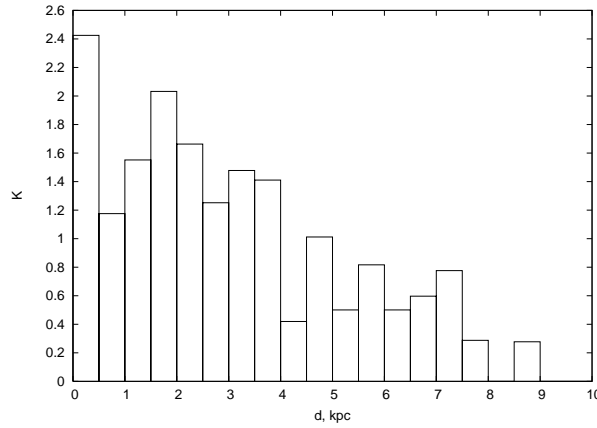


Figure 3: The behaviour of the function $K(d)$, see Eq. (2), for 0.5-kpc intervals.

PSR J0700+ 6418 inside ZEF No. 3 ($d = 0.48$ kpc).

The Geminga pulsar, which is often discussed as a possible source of PeV CRs ($d = 0.16$ kpc) is located at the angular distance $\theta = 3.9^\circ$ from the bottom-right corner of ZEF No. 18.

Remark 6. We do not really need irregular CEF for zones No. 4 and 33 to obtain 80 pulsars in the 2-neighbourhoods of the ZEF. If we exclude them from consideration, the corresponding pulsars move from inside the ZEF to $\theta = 1.7^\circ$ and $\theta = 0.8^\circ$ for ZEF No. 4 and 33 respectively.

As we have stated above, there are 21 ZEF that have pulsars within 2-neighbourhoods. Three more zones (No. 17, 24, and 27, cf. Fig. 1) are added to the list if we select pulsars located at $\theta < 3^\circ$. (In this case, we find 23 more neighbouring pulsars.) An extension of the selection region up to $\theta = 4^\circ$ does not change the list of 'selected' ZEF. Hence, there remain 13 ZEF without neighbouring pulsars and/or galactic SNRs. It is not a simple task to estimate a possible excess of the flux of CRs due to a contribution from a pulsar, see, e.g., [26], but the number of neighbouring pulsars for some of the 'selected' ZEF does not look to be 'sufficient' either. In particular, this applies to huge zones No. 14, 16, and 30 with the first two of them lying in the region with a comparatively big number of EAS per unit cell, see Table 2. Thus we are lead to

the necessity to analyse positions of other possible sources of PeV CRs.

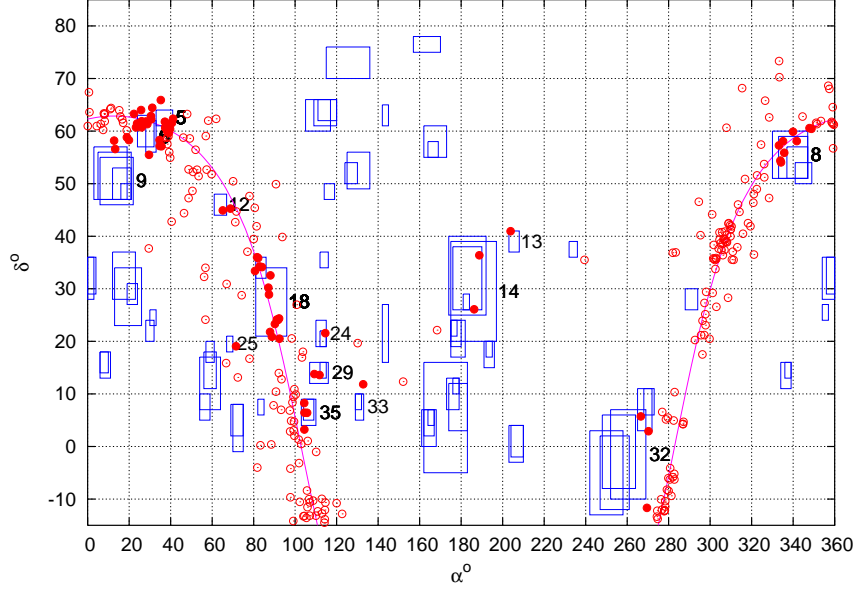


Figure 4: The ZEF and open star clusters () in the region 0 < α < 360. Filled circles denote clusters lying within 2°-neighbourhoods of the ZEF.

4.3. Open Star Clusters and OB-associations. The fact that most open star clusters (OSCs) are dominated by the hottest, i.e., O-type and B-type, giant blue stars made us take a look at positions of these objects. We have analysed coordinates of 299 OSCs that lie in the region 0 < α < 360 and seem to be located in the Milky Way Galaxy. The list of these OSCs was mainly prepared with the use of the SIMBAD database [27]. The result is shown in Fig. 4: 42 OSCs lie inside the ZEF, 32 more clusters are located at angular distances 0 < α < 2° from the ZEF.

Similar to the cases of pulsars and galactic SNRs discussed above, ZEF No. 5, 6, 8, and 18 are among the ‘leaders’ with the biggest number of objects lying within 2°-neighbourhoods. What seems to be more interesting is that the list of ‘selected’ ZEF is now enriched with ZEF No. 12 (OSCs C 0417+448 and NGC 1605), ZEF No. 13 (OSC Czernik 35), and ZEF No. 25 (NGC 1647). In addition, ZEF No. 24, which has the J0751+1807 pulsar at the angular distance α = 2.8°, now gets an object inside (NGC 2420). ZEF No. 15 is added to the list if we extend the selection region up to α = 3°, cf. Fig. 1. In this case, ZEF No. 25 and 26 also obtain a neighbouring OSC, namely the Hyades (C 0424+157). It is worth mentioning that the Hyades is a nearby OSC, located at the distance of about d = 46 pc from the solar system.

It is interesting that ZEF No. 24, 29, and 35, discussed above in connection with the Monogem Ring SNR, contain 1, 2, and 3 OSCs respectively inside. A small cell at the NW corner of ZEF No. 18 also becomes ‘selected’ for the first time. In particular, it contains NGC 1931, M 36, and M 38 inside and M 37 just nearby. (These three Messier objects are located at d = 1.26(1.35 kpc.) Finally, let us mention an OSC that lies near the center of ZEF No. 14. This is the Coma star cluster, located at d = 90 ± 5 pc from the solar system.

Table 4. Parameters of ZEF ‘selected’ by OSCs. See Table 1 for notation.

ZEF	α	δ	N	N	α	D
12	61:::67	44:::48	1857:9	1751:9	33:22	3:19
13	203:::208	37:::41	1280:9	1182:3	29:07	3:39
15	232:::236	36:::39	731:9	657:9	23:60	3:14
25	67:::70	18:::21	115:1	86:6	8:79	3:24

Thus an assumption that open star clusters can be sources of PeV CRs adds three or four more ZEF to the list of zones with neighbouring CR sources. Their parameters are listed in Table 4.

The so-called superbubble model [28] stimulated us to analyse positions of OB-associations. We have found that at least seven OB-associations are located at angular distances $\leq 2^\circ$ from ZEF No. 6, 8, and 36. Three other associations are located at $\leq 2.5^\circ$ from ZEF No. 20. Remarkably, open star clusters and OB-associations taken together with galactic SNRs 'select' all ZEF in the vicinity of the galactic plane.

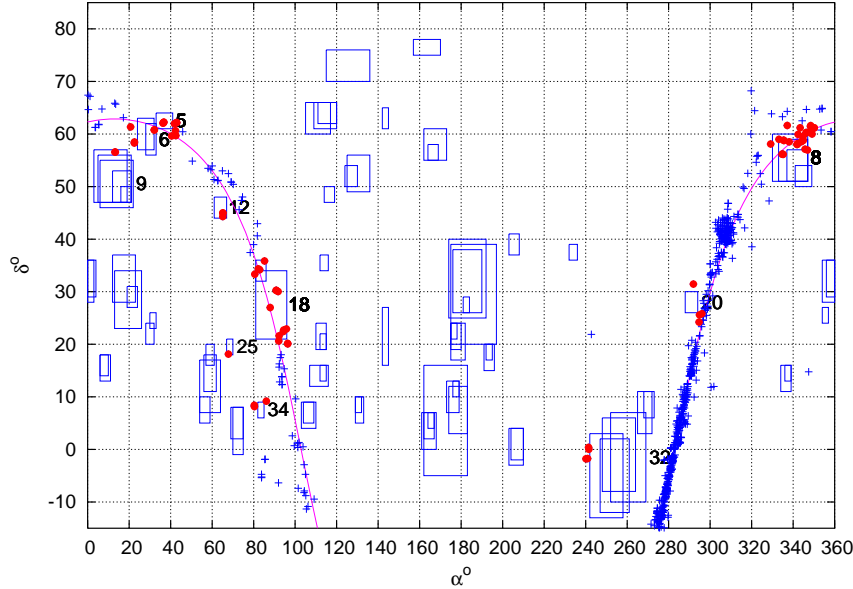


Figure 5: The ZEF and galactic H II regions (+) [29]. Filled circles show regions lying within 2° -neighbourhoods of the ZEF.

4.4. Galactic H II Regions. Another group of astrophysical objects that may be considered as possible sources/accelerators of cosmic rays consists of regions of ionized hydrogen (H II). We have analysed positions of galactic H II regions given in the catalogue by Paladini et al. [29]. The result is shown in Fig. 5.

Seventy-three of 728 H II regions with declination $\geq 15^\circ$ belong to the 2° -neighbourhoods of the ZEF. Thirty-seven of these regions lie inside the corresponding ZEF. The biggest number of H II regions is found in the vicinity of ZEF No. 8 (29 regions, 17 of them inside the zone), ZEF No. 18 (15 and 11 regions respectively), and ZEF No. 5 (9 and 2 regions respectively). Similar to the case of open star clusters, ZEF No. 12 and 25, which do not have any galactic SNRs or pulsars in their vicinity, become 'selected' with respectively three and one H II regions inside. An additional support is also provided to ZEF No. 34 (3 H II regions nearby) and to the small cell in the NW corner of ZEF No. 18. Still, the analysis of positions of galactic H II regions has not added new zones to the list of ZEF with possible sources and/or accelerators of PeV CRs in their vicinity.

An analysis of positions of Wolf-Rayet (WR) stars did not reveal anything remarkable except that there are more than 100 WR stars within the boundaries of a small $5^\circ \times 4^\circ$ cell located inside ZEF No. 16. We shall discuss this fact later. At the moment, we see that 25 of 37 ZEF have at least one galactic object of the types discussed above in their 2° -neighbourhoods, 28 ZEF if we consider 3° -neighbourhoods. Thus, there remain at least 9 ZEF (No. 1, 7, 10, 11, 19, 22, 23, 28, and 37) that do not have known galactic objects of the above types in their vicinity. A number of the zones may look 'underlled'. If we believe that presented ZEF somehow reflect a situation with the angular distribution of the flux of PeV cosmic rays then the appearance of 'empty' and 'underlled' ZEF raises a question on other possible CR sources. An unexpected hint comes from an analysis of arrival directions of the ultra-high energy cosmic rays (UHECRs) registered with the AGASA array.

Earlier, we have used the same data set for a study of arrival times of EAS. In particular, we found 20 groups ('cluster events') of consecutive EAS that produced bursts of the count rate [30], [31]. The majority

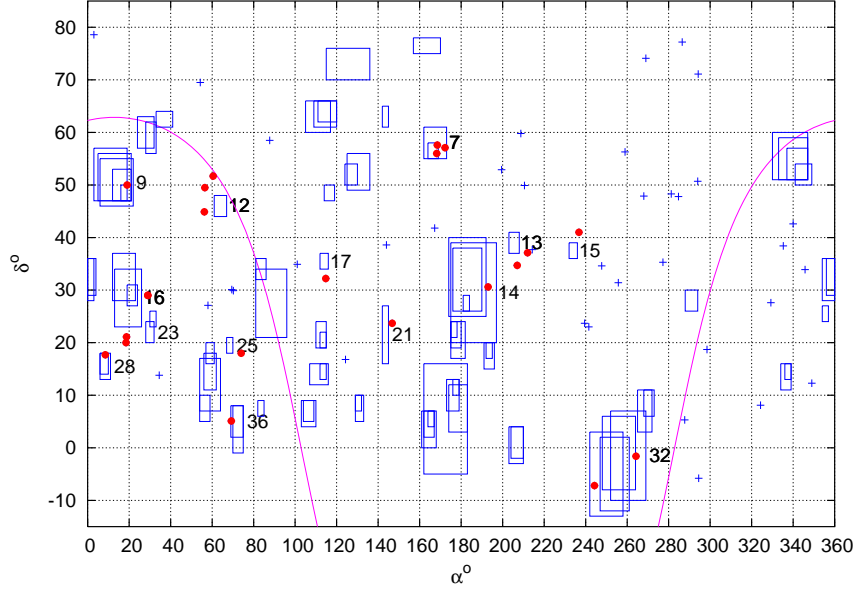


Figure 6: The ZEF and arrival directions of the UHECRs with $E > 4 \cdot 10^9$ eV registered with the AGASA array (+) [15]. Filled circles mark UHECRs lying within 4° -neighbourhoods of the ZEF.

of EAS within these groups did not have close arrival directions but certain clusters covered approximately the same regions of the sky. Surprisingly, we have found a group of four such clusters with the famous AGASA C2' triplet near the center of the corresponding region, see Fig. 30 in [31]. This gave rise to an idea that there may be some connection between UHECRs and cosmic rays in the PeV range. The present investigation gave us a chance to test the idea.

Figure 6 shows arrival direction of 58 UHECRs with energies $E > 4 \cdot 10^9$ eV registered with the AGASA array [15]. Twenty-one of these UHECRs belong to 4° -neighbourhoods of the ZEF. It is remarkable that a number of ZEF that have very few or no neighbouring pulsars and galactic SNRs become 'selected' by the AGASA UHECRs (namely, ZEF No. 7, 12, 17, 23, 25, 28, and 36) with the C2 triplet lying exactly inside ZEF No. 7.² This observation motivated us to compare coordinates of the ZEF with positions of the nearby active galactic nuclei and interacting galaxies (IGs).

4.5. Interacting Galaxies and Active Galactic Nuclei. It has been demonstrated in [33] that a number of particles with energies $E < 10^6$ GeV/nucleon that have had time to arrive to our galaxy from distances greater than 100 Mpc is completely negligible. Thus we restrict our analysis to the sources located at redshift $z \leq 0.01$, which corresponds to $d \leq 40$ Mpc assuming the Hubble constant $H = 75 \text{ km sec}^{-1} \text{ Mpc}^{-1}$. As it will be demonstrated below, in many cases we need far less values of z to find an AGN near a ZEF.

Figure 7 presents positions of the AGN and interacting galaxies at redshifts $z \leq 0.01$. Totally, 60 of 119 AGN that have redshifts $z \leq 0.005$ and are located in the region 17° belong to the 4° -neighbourhoods of the ZEF. Twenty of them lie inside the corresponding ZEF. The same numbers for 249 AGN at redshifts $z \leq 0.01$ are equal to 106 and 32 objects respectively. As for 68 IGs, the corresponding numbers equal 26 and 10, see Table 5 for a list of some of these objects. In its turn, Table 6 presents parameters of ZEF 'selected' by the AGN and interacting galaxies.

Let us discuss these results in more details. First of all, as is clear from Fig. 7, a number of the ZEF cover regions in the vicinity of the Supergalactic plane. ZEF No. 1, 7, 10, 11, 23, 28, and 37, which do not have neighbouring galactic sources of the types discussed above, become 'selected' by the AGN and/or IGs. Further 'support' is provided to ZEF No. 2, 3, 4, 13, 15, and 17. Perhaps, the most exciting observation is

² A recent report by Abbasi et al. [32] has revealed that one of the UHECRs with $E > 3 \cdot 10^{19}$ eV recorded by the HiRes experiment is located at $\alpha = 169.0$ and $\delta = 55.9$ and thus also lies inside ZEF No. 7.

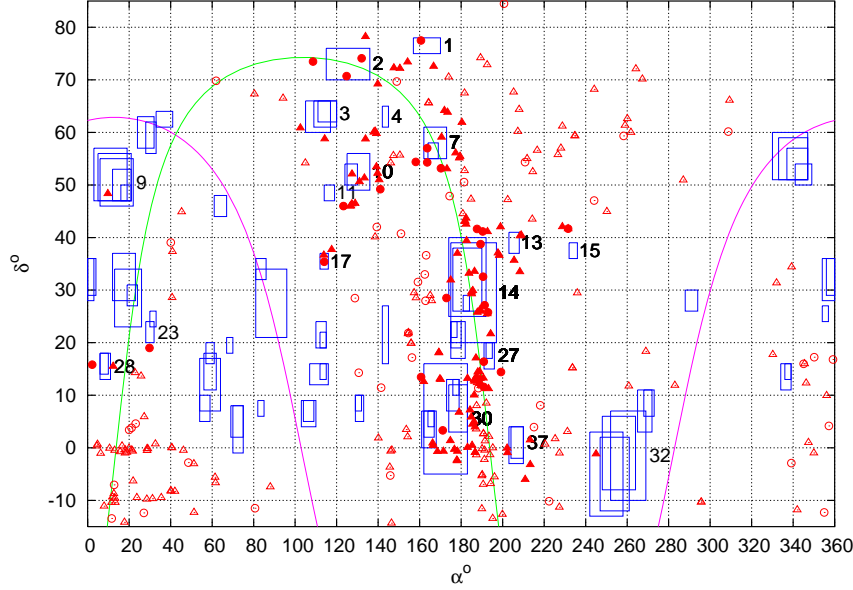


Figure 7: The ZEF, AGN (\blacktriangle), and interacting galaxies (\circ) at redshift $z \approx 0.01$ [27]. Filled triangles and open circles mark respectively AGN and IGs that lie within 4° -neighbourhoods of the ZEF. The \sim -like curve shows the Supergalactic plane.

that there are numerous AGN and IGs within and near huge but ‘under filled’ zones No. 14 and 30 with a whole bunch of galaxies located between ZEF No. 27 and No. 30. In sum, ZEF No. 14 has 23 neighbouring AGN and 8 IGs with respectively 19 and 7 of them at redshifts $z < 0.005$. Twenty-nine AGN and 2 IGs belong to the 4° -neighbourhood of ZEF No. 30. Fourteen of these AGN and both IGs have $z < 0.005$. Finally, all three IGs and 8 of 11 AGN that lie in the 4° -neighbourhood of ZEF No. 27 are located at redshifts $z < 0.005$ (with the M 58 galaxy at $z = 0.005047$). What seems to be even more important is that almost all galaxies selected as being close to ZEF No. 27 belong to the Virgo cluster of galaxies. These are NGC 4762, NGC 4550, NGC 4639, NGC 4477, M 58, M 88, M 89, M 90, M 91 with the famous M 87 galaxy located at $\alpha = 4:1$ from ZEF No. 27. Galaxies M 84, NGC 4380, and NGC 4438, which also belong to the Virgo cluster, lie closer to ZEF No. 30. Remarkably, NGC 4380 is a BL Lac object. In addition, one can notice that the Coma cluster and Coma supercluster of galaxies lie inside ZEF No. 14. (Their coordinates are $\alpha = 195^\circ$, $\delta = 28^\circ$ and $\alpha = 186^\circ$, $\delta = 24^\circ$ respectively [36].) In our opinion, all this makes a basis for a conjecture that zones No. 30, 27, 14, and possibly No. 13 may be considered as parts of one huge ZEF, which to big extent originates from a contribution to the overall CR flux from the Coma/Virgo cluster of galaxies.

As we have already mentioned above, AGN and IGs provide additional ‘support’ to comparatively large ZEF No. 2 and No. 3 ‘selected’ by pulsars but ‘select’ a large zone No. 37 for the first time. On the other hand, it is hard to believe that AGN and/or IGs or even their compact groups can produce small ZEF of CRs in the PeV region as those No. 4, 11, 13, 15, 17, 23, and 28. It seems more likely that these ZEF should originate from a contribution from galactic sources. Still, we have seen that ZEF No. 11, 23, and 28 do not have neighbouring objects of the types considered above. The same is true for ZEF No. 7. Besides this, one cannot help mentioning that ZEF No. 7, 13, 15, 17, and 28 are ‘selected’ by both the UHECRs registered with the AGASA array on the one hand and AGN and IGs (except for ZEF No. 13) on the other. Thus we are lead to the following conjectures: (i) the corresponding UHECRs originate from the AGN selected in the neighbourhoods of these ZEF, (ii) a part of UHECRs are neutral particles or there are certain voids in intergalactic magnetic fields, (iii) a part of ZEF, especially those far from the galactic plane, are formed with a contribution of extragalactic CRs.

Notice also that another AGASA UHECR lies inside ZEF No. 14 and has a number of AGN around, cf. Figures 6 and 7. On the other hand, three other AGASA UHECRs lie within ZEF No. 9 and 32, which have numerous pulsars inside but just one AGN each, both located comparatively far from the arrival directions of the UHECRs. In our opinion, this fact may witness in favour of an idea that a part of UHECRs may

Table 5. A list of some AGN and interacting galaxies (IGs) located at redshifts $z < 0.01$ and lying within 4 $^{\circ}$ -neighbourhoods of the ZEF. Types of the AGN: 'Sy' is for Seyfert galaxies, possibly with their type (1 or 2), 'LINER' is for Low-Ionization Nuclear Emission-line Regions, and 'BLL' is for a BL Lac object. For ZEF with nearby AGN, the number of nearby AGN at redshifts $z < 0.005$ and $z < 0.01$ respectively are given in parenthesis. Names of AGN beginning with 'J' correspond to the Veron-Cetty & Veron catalogue [34]. For IGs, we give nomenclature used in the SIMBAD database [27] with data given according to [35].

ZEF				Name	Type	z
1 (1/4)	147:59	72:28	3:79	NGC 2985	Sy1	0:004306
	160:66	77:49	0:00	APG 156	IG	0:006274
2 (3/3)	139:83	69:20	1:55	NGC 2787	LINER	0:002298
	124:77	70:72	0:00	APG 268	IG	0:000524
3 (0/2)	114:24	58:77	1:23	Mrk 9	Sy1	0:006321
	102:54	60:85	1:20	NGC 2273	Sy2	0:006151
4 (2/3)	137:91	60:04	2:23	NGC 2768	Sy	0:004590
7 (7/8)	173:14	53:07	1:93	NGC 3718	LINER	0:003306
	170:57	59:07	0:00	NGC 3642	LINER	0:005327
10 (6/11)	133:39	51:31	0:00	NGC 2681	LINER	0:002308
	133:90	58:73	2:73	NGC 2685	Sy2	0:002915
11	123:31	45:99	3:13	APG 6	IG	0:001491
13 (3/6)	205:53	35:65	1:35	NGC 5273	Sy1	0:003596
	198:96	42:03	3:20	M 63	LINER	0:001678
14 (19/23)	194:18	21:68	0:00	M 64	Sy	0:001341
	185:03	29:28	0:00	NGC 4278	LINER	0:002145
	186:45	33:55	0:00	NGC 4395	Sy1	0:001061
	192:72	41:12	1:25	M 94	Sy	0:001024
	189:34	38:75	0:00	APG 211	IG	0:001484
	190:38	41:15	1:15	APG 23	IG	0:001811
15 (0/2)	231:53	41:67	2:69	NGC 5929	LINER	0:008912
	228:76	42:05	3:92	NGC 5899	LINER	0:008503
17	113:99	35:38	0:00	APG 250	IG	0:004543
23	29:83	19:01	0:99	NGC 772	IG	0:008199
27 (8/11)	188:88	12:22	3:46	NGC 4550	LINER	0:001338
	188:92	12:56	3:17	M 89	Sy2	0:000914
	189:21	13:16	2:53	M 90	Sy	0:000721
	188:86	14:50	2:13	M 91	LINER	0:001644
28 (0/1)	12:27	15:49	1:22	J004903.7+152907	Sy1	0:010
	2:19	15:82	3:66	APG 235	IG	0:002885
30 (14/29)	178:16	2:47	0:00	Mrk 1307	Sy1	0:003426
	186:34	10:02	3:29	NGC 4380	BLL	0:003229
	161:96	12:58	0:04	M 105	LINER	0:002922
	186:27	12:89	3:18	M 84	Sy2	0:003369
	170:06	12:99	0:00	M 66	LINER	0:002425
	186:94	13:01	3:84	NGC 4438	LINER	0:000234
37 (0/5)	169:73	13:09	0:00	M 65	LINER	0:002692
	213:31	3:21	3:31	NGC 5506	Sy2	0:006068
	202:34	0:94	0:66	J132921.3 005639	Sy1	0:010

originate from pulsars located in the Galaxy. This idea has already been discussed elsewhere, see, e.g., [37] and references therein.

4.6. ZEF No. 16. Finally, let us briefly discuss ZEF No. 16. Recall that this ZEF has just one distant pulsar

Table 6. Parameters of ZEF ‘selected’ by AGN and interacting galaxies at redshifts $z < 0.01$. See Table 1 for notation.

ZEF			N	N		D
1	157 :::170	75 :::78	1151:3	1036:5	35:80	3:21
7	162 :::173	55 :::61	4908:3	4688:6	69:51	3:16
	164 :::169	55 :::58	1177:3	1089:2	27:86	3:16
10	124 :::130	50 :::54	1945:7	1818:6	36:91	3:44
	125 :::136	49 :::56	5984:6	5793:9	59:34	3:21
11	114 :::119	47 :::50	1223:3	1127:1	30:18	3:19
23	28 :::32	20 :::24	263:0	223:6	11:95	3:30
	30 :::33	23 :::26	209:2	171:3	12:10	3:13
28	6 :::10	14 :::18	115:1	84:9	9:03	3:35
	6 :::11	13 :::18	159:1	121:2	10:48	3:62
37	203 :::210	3 :::4	11:2	4:5	1:97	3:42
	204 :::210	2 :::4	10:3	3:7	1:73	3:85

at its left border, see Fig. 2, and no other potential sources of CRs nearby but more than 100 WR stars located inside its small central cell. (Also notice that there is an AGASA UHECR located to the right of ZEF No. 16, see Fig. 6.) Still, the zone lies in the Supergalactic plane. A key to a possible explanation of the appearance of ZEF No. 16 comes from an observation that all these WR stars belong to the M 33 galaxy, a prominent member of the Local Group of galaxies ($\alpha = 23^h 46^m$, $\delta = 30^\circ 66'$; $d = 730 \pm 168$ kpc [38]). What seems to be really important is that M 33 hosts the most luminous steady X-ray source in the Local Group, see [39] and references therein, a number of radio sources, and more than 80 H II regions [36] including NGC 588, NGC 595, and NGC 604, a giant diffuse nebula, nearly 1500 light-years across. Thus we expect that ZEF No. 16 may originate from a contribution from these objects.

Interestingly, one of successive air shower events in the 50 TeV {10 PeV energy range reported by the LAAS group [40] has the averaged ‘coordinates’ $\alpha = 21^h 75^m$, $\delta = 30^\circ 81'$ and thus also lies within the central cell of ZEF No. 16.

4.7. ‘Empty’ ZEF. We are thus left with two ZEF without any object of the types discussed above in their vicinity. These are ZEF No. 19 and 22. There naturally appears a question of why are they ‘empty’?

Table 7. Parameters of ‘empty’ ZEF No. 19 and 22.

ZEF			N	N		D
19	354 :::363	28 :::36	2927:9	2809:5	38:15	3:10
	356 :::364	29 :::36	2377:0	2267:3	34:95	3:14
22	354 :::357	24 :::27	233:5	190:3	13:56	3:19

Both ‘empty’ ZEF are made of regular cells. (They join into one bigger cell if we consider irregular cells.) Parameters of these two ZEF are listed in Table 7. One can see that there is nothing special, perhaps excluding the fact that the values of deviation D are close to the lowest allowed boundary. Still, this is not unusual for non-empty ZEF either, as is clear from Tables 1{4 and 6. It is possibly more important that ZEF No. 19 intersects the boundary $\alpha = 360^\circ$, and ZEF No. 22 lies close to it. At the moment, we cannot completely exclude a possibility that the appearance of ZEF No. 19 and 22 is an artifact of the algorithm resulting from a boundary effect. It is remarkable though that two of the eleven point sources in the 100 GeV to 100 TeV energy range with an excess greater than 4 σ , reported recently by the Milagro Collaboration [41] are located inside ZEF No. 19. In addition, averaged coordinates of another successive air shower event reported by the LAAS group [40] lie within the boundaries of ZEF No. 19.

5. EAS with $N_e \approx 2 \cdot 10^5$

It is undoubtedly interesting to compare arrival directions of CRs with energies just below the knee with those above it. Unfortunately, as we have already explained in Sec. 2, the data set under consideration

mostly covers the interval of energies just below the knee. Still, we find it interesting to perform a brief analysis of arrival directions of 142,223 EAS with $\alpha_0 = 45^\circ$ and $N_e = 2 \cdot 10^5$, which corresponds to energies $E > 2 \cdot 10^6$ eV.

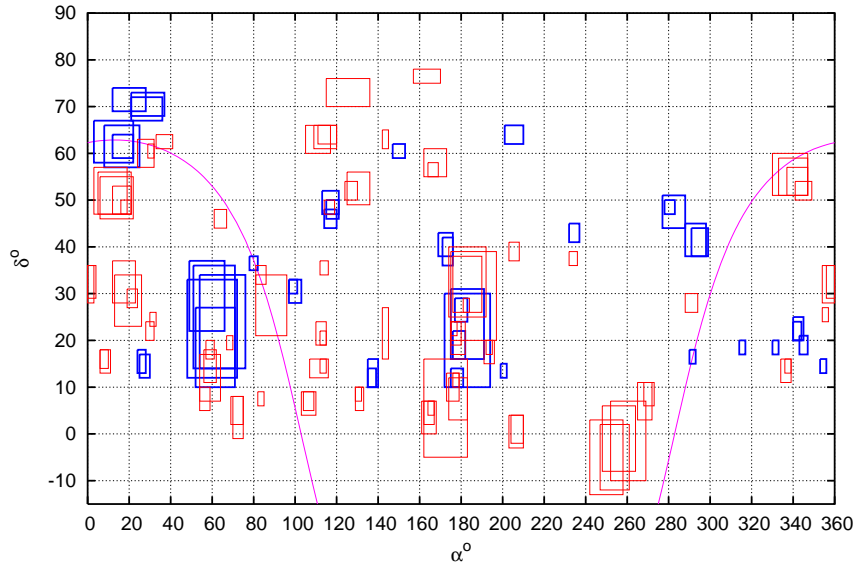


Figure 8: Mutual positions of the ZEF obtained for the whole data set and for EAS with $N_e = 2 \cdot 10^5$ (rectangles in thin and thick lines respectively.)

After applying the same procedure of data analysis (with the same random seeds used at the stage of the data alignment) we are left with 111,370 EAS and 21 new ZEF combined of 147 regular cells, see Fig. 8. We do not think that $1.1 \cdot 10^5$ showers are sufficient to make definite conclusions on a distribution of their arrival directions and will thus only give brief comments.

First of all, one can see that there is a huge new ZEF that partially overlaps with old ZEF No. 14, 27, and 30. This new ZEF includes all AGN and IGs selected earlier that belong to the Virgo cluster of galaxies and those in the region of the Coma cluster. It seems to be quite natural since one may expect that AGN normally produce more energetic particles than pulsars and SNRs. Next, there is another huge ZEF which includes old ZEF No. 25 and a part of ZEF No. 26. This ZEF occurs to be mostly filled with OSCs and pulsars. One can also see a ZEF that is approximately adjacent to ZEF No. 6 and 9. Both SNRs located near the top left corner of ZEF No. 6 (G126.2+1.6 and G127.1+0.5) belong to this new ZEF. Besides this, it also contains the famous Tycho SNR (SN1572). There are also a number of other new ZEF that lie close to the old ones. Finally, one can see a number of new ZEF that occupy areas of their own. All new ZEF have these or that astrophysical objects of the types discussed above in their vicinity.

6. Conclusions

We have presented the results of an analysis of arrival directions of more than 10^6 EAS in the energy range $0.1\text{--}10$ PeV registered with the EAS1000 Prototype Array. An iterative algorithm developed for this investigation allowed us to find a number of zones with an excess of CR flux in the data set under consideration at 3σ level. The zones are mostly located in the vicinity of the galactic and Supergalactic planes. The majority of the ZEF have powerful galactic sources of CRs inside or nearby, namely, SNRs (with the Crab Nebula, Cassiopeia A, and the Monogem Ring among them), pulsars, open star clusters, OB-associations, and regions of ionized hydrogen. This observation seems to witness in favour of the traditional point of view that objects of all these types make a contribution to the flux of PeV cosmic rays.

On the other hand, there are a number of ZEF that have none or just a few objects of the above types in their vicinity. We find that one of such ZEF contains the M33 galaxy inside, while the majority of others have neighbouring active galactic nuclei and/or interacting galaxies at redshifts $z < 0.01$ with a big group of them

located in the Virgo cluster of galaxies. These observations together with a number of coincidences between arrival directions of UHECRs with $E > 4 \cdot 10^9$ eV registered with the AGASA array and positions of some ZEF lead us to the following conjectures: (i) the flux of PeV cosmic rays is a superposition of two components, a galactic and an extragalactic ones (cf. [11]), and at least a part of the extragalactic component ‘remembers’ its origin; (ii) cosmic rays in the PeV (and possibly higher) energy range originate from astrophysical objects of various types; (iii) there are astrophysical sources that emit/accelerate particles in a wide range of energies so that a part of both PeV and EeV cosmic rays may have common origin. (This is not a new idea. One can find a number of models which attempt to explain the origin of CRs of very different energies with the help of a unique type of sources and/or mechanism, see, e.g., [28], [42], [9], and [10].) It may be rather difficult though to explain how extragalactic sources can form a noticeable flux of PeV CRs from directions close to their origin. Perhaps, the most obvious ideas are that at least a part of the extragalactic component consists of neutral particles or that there are certain voids in intergalactic magnetic fields.

The presented results pose a number of tasks for the future investigation. First of all, it is desirable to perform a comprehensive analysis of the algorithm with the use of a Monte-Carlo simulation. This may help one to figure out what kind of excess of the CR flux is detected and which is not. In particular, this may help to explain why an excess of cosmic ray flux is detected in direction to certain possible CR sources while to others it is not. Next, it is desirable to study arrival directions of CRs just above the knee with greater statistics. To implement this task, we plan to use the data obtained in late 1980’s with the EASMSU Array and to employ another data set already obtained with the EAS-1000 Prototype Array. Finally, we also plan to study another interesting feature of the CR arrival directions revealed during the investigation. These are zones with ‘depressed’ flux, i.e., zones with a number of EAS much less than the average. We think that an analysis of such ‘sinks’ can provide some information useful for understanding the origin of cosmic rays in the energy range near the knee.

Acknowledgments

We thank A.A.Chilingarian, A.D.Erlykin, and E.Parizot for useful and stimulating communications. The whole investigation would have been impossible without our colleagues who obtained the experimental data. M.Z. thanks A.Golubin, A.Habib-ur-Rahman-Khan, V.Lebedev, I.Sinelbov, and R.Zhukov for the nice PC, which has done the main work, and B. and C.Woodworth for the enlightening discussion.

This research has made intensive use of the NASA/IPAC Extragalactic Database (NED), which is operated by the Jet Propulsion Laboratory, California Institute of Technology, under contract with the National Aeronautics and Space Administration, resources provided by SEDS [43], and especially the SIMBAD database, operated at CDS, Strasbourg, France.

Only free, open source software has been used for the investigation.

References

- [1] V.F. Hess, Phys. Z. 13 (1912) 1084.
- [2] A. Chilingarian et al., \Detection of the high-energy cosmic rays from the Monogem Ring," *Astrophys. J.* 597 (2003) L129.
- [3] T. Antoniet al. for the KASCADE Collaboration, \Large scale cosmic-ray anisotropy with KASCADE," *Astrophys. J.* 604 (2004) 687. Available from arXiv:astro-ph/0312375.
K.H. Kampert et al., \Cosmic rays in the knee'-region. Recent results from KASCADE," *Acta Phys. Polon. B* 35 (2004) 1799. Available from arXiv:astro-ph/0405608.
- [4] G. Benko et al., \Search for Sources of Primary Cosmic Rays at Energies Above 0.1 PeV at Tien Shan," *Izv. RAN, Ser. Fiz.* 69 (2004) 1599. Available from arXiv:astro-ph/0502065.
- [5] V.A. Kozaryivsky et al., \Mean diurnal variations of cosmic ray intensity as measured by AndyrchiA ir Shower Array," arXiv:astro-ph/0406059.
- [6] R.W. Clay et al., \Anisotropies between 10^{14} eV and 10^{18} eV," *Proc. 25th ICRC, Durban, 1997*, 4, 185.
- [7] G.V. Kulikov, G.B. Khristiansen, *Zh. Eksp. Teor. Fiz.* 35 (1958) 635.
- [8] E. Roulet, \Astroparticle Theory: Some New Insights into High Energy Cosmic Rays," *Int. J. Mod. Phys. A* 19 (2004) 1133. Available from arXiv:astro-ph/0310367.
- [9] S.D. Wick, C.D. Demmer, A. Atoyan, \High-Energy Cosmic Rays from Gamma-Ray Bursts," *Astropart. Phys.* 21 (2004) 125. Available from arXiv:astro-ph/0310667.
- [10] A. Dar, \The Origin of Cosmic Rays | A 96-Year-Old Puzzle Solved?," arXiv:astro-ph/0408310.
- [11] H. Muraishi, S. Yanagita, T. Yoshida, \Galactic modulation of extragalactic cosmic rays: Possible origin of the knee in the cosmic ray spectrum," arXiv:astro-ph/0502132; v.2.
- [12] T.K. Gaisser, \Origin of cosmic radiation," *AP Conf. Proc.* 558 (2001) 27. Available from arXiv:astro-ph/0011524.
- [13] A.D. Erlykin, A.W. Wolfendale, \A single source of cosmic rays in the range 10^{15} – 10^{16} eV," *J. Phys. G: Nucl. Part. Phys.* 23 (1997) 979.
| , \Structure in the cosmic ray spectrum: an update," *J. Phys. G: Nucl. Part. Phys.* 27 (2001) 1005.
- [14] S.E. Thorsett et al., \Pulsar PSR B0656+14, the Monogem Ring, and the origin of the knee' in the primary cosmic ray spectrum," *Astrophys. J.* 592 (2003) L71. Available from arXiv:astro-ph/0306462.
- [15] N. Hayashida et al., \Updated AGASA event list above 4×10^{19} eV," *Astrophys. J.* 522 (1999) 225. Available from arXiv:astro-ph/0008102.
- [16] Yu.A. Fomin et al., \New results of the EAS-1000 Prototype operation," *Proc. 26th ICRC, Salt Lake City, 1999*, 1, 286.
- [17] L. Sun, S. Sun, \The cosmic ray incident directions observed from the Northern and Southern hemispheres," *Proc. 25th ICRC, Durban, 1997*, 4, 165.
- [18] J.W. Eaton, GNU Octave: A High-Level Interactive Language for Numerical Computations, Edition 3 for version 2.0.13, 1997. (<http://www.octave.org/>)
- [19] D.A. Green, \A Catalogue of Galactic Supernova Remnants (2004 January version)," *Mullard Radio Astronomy Observatory, Cavendish Laboratory, Cambridge, United Kingdom* (available at <http://www.mrao.cam.ac.uk/surveys/snrs/>); see also D.A. Green, \Galactic Supernova Remnants: an Updated Catalogue and Some Statistics," *Bull. Astron. Soc. India* 32 (2004) 335. Available from arXiv:astro-ph/0411083.
- [20] H.J. Volk, \TeV gamma-ray observations and the origin of cosmic rays III," arXiv:astro-ph/0312585.
- [21] E.G. Berezhko, H.J. Volk, \Direct evidence of efficient cosmic ray acceleration and magnetic field amplification in Cassiopeia A," arXiv:astro-ph/0404203.
- [22] T. Kobayashi et al., \High energy cosmic-ray electrons beyond 100 GeV," *Proc. 26th ICRC, Salt Lake City, 1999*, 3, 61.
K. Yoshida et al., \The origin of high energy cosmic-ray electrons and nearby supernova remnants," *Proc. 28th ICRC, Tsukuba, 2003*, 1, 1993.
- [23] A.D. Erlykin, A.W. Wolfendale, \The origin of the knee in the cosmic-ray energy spectrum," arXiv:astro-ph/0103477.
- [24] The ATNF Pulsar Database, <http://www.atnf.csiro.au/research/pulsar/psrcat/>; see also: R.N. Manchester, G.B. Hobbs, A. Teoh, M. Hobbs, \The ATNF Pulsar Catalogue," arXiv:astro-ph/0412641.

- [25] J.H. Taylor, J.M. Cordes, *Astrophys. J.* 411 (1993) 674.
- [26] A.D. Erlykin, A.W. Wolfendale, \Cosmic rays and the Monogenic supernova remnant," *Astropart. Phys.* 22 (2004) 47. Available from [arXiv:astro-ph/0404530](http://arxiv.org/abs/astro-ph/0404530).
- [27] The SIMBAD database, <http://simbad.u-strasbg.fr/Simbad>
- [28] E. Parizot, \Superbubbles & the Galactic evolution of ^6Li , Be and B," *Astron. Astrophys.* 362 (2000) 786.
E. Parizot, A. Marcowith, E. van der Swaluw, A.M. Bykov, V. Tatischev, \Superbubbles and Energetic Particles in the Galaxy. I: Collective effects of particle acceleration," [arXiv:astro-ph/0405531](http://arxiv.org/abs/astro-ph/0405531).
E. Parizot, \Cosmic-rays: an unsolved mystery at all energies!," [arXiv:astro-ph/0501274](http://arxiv.org/abs/astro-ph/0501274).
- [29] R. Paladini et al., \A radio catalog of Galactic H II regions for applications from decimeter to millimeter wavelengths," *Astron. & Astrophys.* 397 (2003) 213.
- [30] O.V. Vedeneev et al., \EAS clusters with $N_e \approx 5 \times 10^4$," *Izv. Ros. Akad. Nauk, Ser. Fiz.* 65 (2001) 1674.
- [31] Yu.A. Fomin et al., \Clusters of EAS with electron number $> 10^4$," Preprint SINP MSU 2002-9/693. Available from [arXiv:astro-ph/0203478](http://arxiv.org/abs/astro-ph/0203478).
- [32] R.U. Abbasi, T. Abu-Zayyad, J.F. Amann et al., \Search for Point Sources of Ultra-High Energy Cosmic Rays Above 40 EeV Using a Maximum Likelihood Ratio Test," [arXiv:astro-ph/0412617](http://arxiv.org/abs/astro-ph/0412617).
- [33] G. Tarle et al., \Limitations of the transport of cosmic ray antimatter from distant galaxies," *Proc. 25th ICRC*, Durban, 1997, 4, 205.
- [34] M.P. Veron-Cetty, P. Veron, \Quasars and Active Galactic Nuclei," *Astron. & Astrophys.* 412 (2003) 399.
- [35] H. Arp, \Atlas of peculiar galaxies," *Astrophys. J., Suppl. Ser.* 14 (1966) 1.
- [36] The NASA/IPAC Extragalactic Database, <http://nedwww.ipac.caltech.edu/index.html>
- [37] M. Takeda et al., \Small-scale anisotropy of cosmic rays above 10^{19} eV observed with the Akeno Giant Air Shower Array," *Astrophys. J.* 522 (1999) 225. Available from [arXiv:astro-ph/9902239](http://arxiv.org/abs/astro-ph/9902239).
- [38] A. Bunthaler, M.J. Reid, H. Falcke, L.J. Greenhill, C. Henkel, \The Geometric Distance and Proper Motion of the Triangulum Galaxy (M33)," *Science* 307 (2005) 1440. Available from [arXiv:astro-ph/0503058](http://arxiv.org/abs/astro-ph/0503058).
- [39] G. Dubus et al., \High resolution Chandra X-ray imaging of the nucleus of M33," [arXiv:astro-ph/0406310](http://arxiv.org/abs/astro-ph/0406310).
- [40] N. Ochi, T. Wada, Y. Yamashita et al., \Anisotropy of Successive Air Showers," *Nucl. Phys. B (Proc. Suppl.)* 97 (2001) 173.
- [41] P.M. Saz Parkinson for the Milagro Collaboration, \Detection of TeV gamma-rays from extended sources with Milagro," [arXiv:astro-ph/0503244](http://arxiv.org/abs/astro-ph/0503244).
- [42] A.D. Erlykin, T. Wibig, A.W. Wolfendale, \A universal origin for cosmic rays above 10^7 GeV?," *New Journal of Physics* 3 (2001) 18.1. (<http://www.njp.org/>)
- [43] Students for the Exploration and Development of Space (SEDS), available at <http://www.seds.org/>.